JGR Oceans

RESEARCH ARTICLE
10.1029/2020JC016565

Special Section:
The Arctic: An AGU Joint Special Collection

Summer High-Wind Events and Phytoplankton Productivity in the Arctic Ocean

Alex D. Crawford[1], Kristen M. Krumhardt[2], Nicole S. Lovenduski[3], Gert L. van Dijken[4], and Kevin R. Arrigo[4]

[1]Department of Earth Sciences, The College of Wooster, Wooster, OH, USA, [2]Climate and Global Dynamics Laboratory, National Center for Atmospheric Research, Boulder, CO, USA, [3]Department of Atmospheric and Oceanic Sciences and Institute of Arctic and Alpine Research, University of Colorado Boulder, Boulder, CO, USA, [4]Department of Earth System Science, Stanford University, Stanford, CA, USA

Abstract At the base of the marine food web, phytoplankton are an essential component of the Arctic Ocean ecosystem and carbon cycle. Especially after sea ice retreats and light becomes more available to the Arctic Ocean each summer, phytoplankton productivity is limited by nutrient availability, which can be replenished by vertical mixing of the water column. One potential mixing mechanism is gale-force wind associated with summer storm activity. Past studies show that sustained high winds (>10 m s^{-1}) impart sufficient stress on the ocean surface to induce vertical mixing, and it has been speculated that greater storm activity may increase net primary productivity (NPP) on a year-to-year timescale. We test this idea using a combination of satellite products and reanalysis data from 1998 to 2018. After controlling for the amount of open water, sea-surface temperature, and wind direction, we find evidence that greater frequency of high-wind events in summer is associated with greater seasonal NPP in the Barents, Laptev, East Siberian, and southern Chukchi Seas. This relationship is only robust for the Barents and southern Chukchi Seas, which are more strongly impacted by inflow of relatively nutrient-rich water from the Atlantic and Pacific Oceans, respectively. In other words, stormier summers may have higher productivity in several regions of the Arctic Ocean, but especially the two inflow seas. Additionally, a recent rise in high-wind frequency in the Barents Sea may have contributed to the simultaneous increase in NPP.

Plain-Language Summary Microscopic phytoplankton are an essential component of the Arctic Ocean ecosystem because they are the base of the marine food web. Sea ice in the Arctic Ocean limits phytoplankton growth by reducing how much sunlight reaches the ocean surface, but sea ice is becoming less common in the Arctic Ocean over time. This increases the importance of another limit on phytoplankton: nutrients. Phytoplankton near the surface use up nutrients rapidly in spring, so summer growth is limited by the rate that nutrients are replenished. Past studies have shown that individual storms with strong winds can stir up enough nutrients from deeper waters to temporarily enhance phytoplankton activity. We find that this is not simply a localized or short-term impact. Stormier summers tend to have higher productivity in several regions of the Arctic Ocean. We also find that the frequency of high-wind events has increased in recent years, so although the decline in Arctic sea ice can explain much of the increase in phytoplankton growth over 1998–2018, an increase in storminess is also a likely part of the story.

Key Points:
- Past studies suggest that wind-induced mixing enhances Arctic Ocean phytoplankton productivity by increasing nutrient availability
- Greater frequency of summer high-wind events is associated with enhanced NPP in the two inflow seas (Barents Sea and southern Chukchi Sea)
- Positive trend of NPP for the Barents Sea in recent years is partly explained by increased frequency of high-wind events

Supporting Information:
- Supporting Information S1

Correspondence to:
A. D. Crawford,
acrawford@wooster.edu

Citation:
Crawford, A. D., Krumhardt, K. M., Lovenduski, N. S., van Dijken, G. L., & Arrigo, K. R. (2020). Summer high-wind events and phytoplankton productivity in the Arctic Ocean. *Journal of Geophysical Research: Oceans*, *125*, e2020JC016565. https://doi.org/10.1029/2020JC016565

Received 2 JUL 2020
Accepted 13 AUG 2020
Accepted article online 18 AUG 2020

1. Introduction

As summer Arctic sea ice extent has declined over the past several decades (Serreze & Meier, 2018; Stroeve et al., 2012) the period of ice-free conditions has lengthened by a few weeks to months throughout much of the Arctic Ocean (Peng et al., 2018; Stroeve et al., 2016; Figure 1). Studies suggest that this ice decline has affected various aspects of the Arctic physical environment, from amplification of Arctic warming in autumn/winter (Serreze & Barry, 2011; Yim et al., 2016) to enhanced wave activity (Thomson et al., 2016) to shifting habitats for marine species (Kovacs et al., 2010; Wassmann et al., 2011).

At the base of the Arctic marine food web, unicellular photosynthesizing phytoplankton are particularly sensitive to changing environmental conditions (Codispoti et al., 2013; Ji et al., 2013; Wang et al., 2005). Productivity by phytoplankton makes energy available to higher trophic levels in marine food webs (Hays et al., 2005); thus, any change to net primary productivity (NPP) may have cascading effects on Arctic

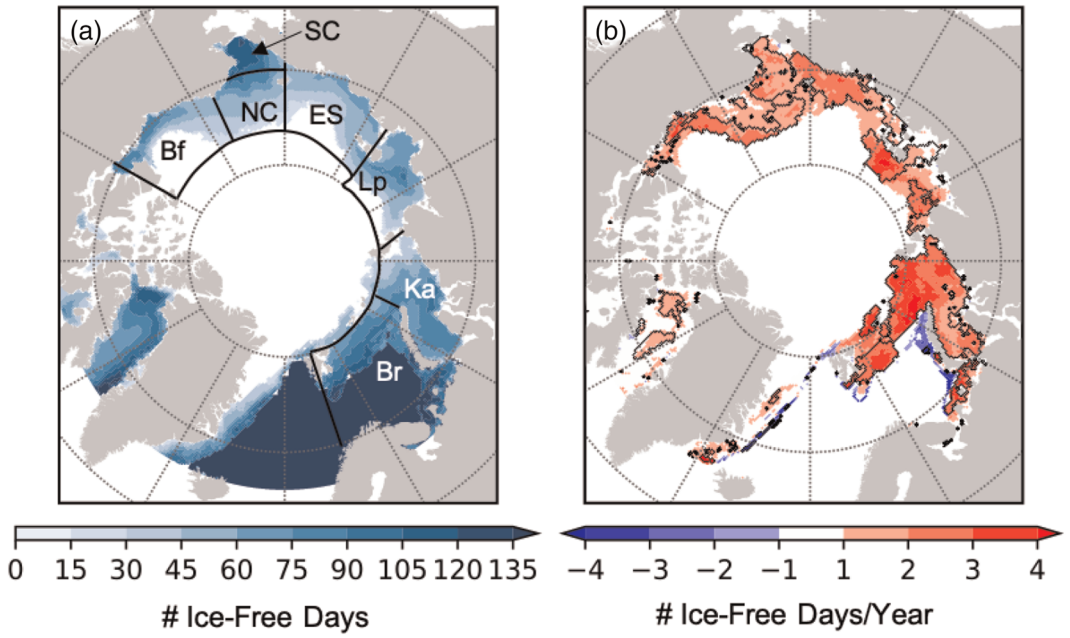

Figure 1. (a) Average length of continuous ice-free period (SIC < 10%) for 1998–2018. The marginal seas examined in this study include the Beaufort (Bf), the southern and northern Chukchi (SC & NC), East Siberian (ES), Laptev (Lp), Kara (Ka), and Barents (Br) Seas. (b) Trend in ice-free period from 1998 to 2018. Black contour indicates significant trends at $p < 0.05$. Grid cells with fewer than 15 years of nonzero data are masked.

marine ecosystems (Cheung et al., 2010; Pörtner et al., 2014). The seasonal cycle of Arctic marine NPP is dictated by the supply of light and nutrients to the upper ocean (Carmack et al., 2006; Popova et al., 2010; Tremblay & Gagnon, 2009). During winter months, insolation is either absent or too weak for photosynthesis to occur (Popova et al., 2010). When insolation increases in spring, some light reaches the ocean surface in leads (Assmy et al., 2017) or through thinner ice, especially when ice exhibits a high melt pond fraction (Hudson et al., 2013). This light is sufficient for low-light-adapted phytoplankton to grow beneath sea ice over 100 km from the ice edge (Arrigo et al., 2012, 2014; Kauko et al., 2019; Mundy et al., 2014). Although some phytoplankton species grow beneath the sea ice, many others bloom along the ice edge (Frey et al., 2011; Perrette et al., 2011; Renaut et al., 2018). The importance of light limitation is also evidenced by greater annual NPP in areas that are permanently open water compared to those that are seasonally ice-covered (Wassmann et al., 2010). Additionally, Arctic NPP has increased as sea ice cover has declined (Arrigo et al., 2008; Arrigo & van Dijken, 2011, 2015; Bélanger et al., 2013).

Whether under the sea ice or along the ice edge, spring blooms often end when nutrients (especially nitrate) in surface waters are fully consumed (Codispoti et al., 2013; Popova et al., 2010). Therefore, summer NPP is strongly linked to nutrient availability (Oziel et al., 2017; Tremblay et al., 2006; Tremblay & Gagnon, 2009). Additionally, both observational and modeling results suggest a dominant role for nutrient availability in driving changes in NPP. Lewis et al. (2020) found that although an increasing ice-free area can explain most of the increase in Arctic NPP from 1998 to 2008, the continued increase of NPP from 2009 to 2018 is more closely related to an increase in phytoplankton biomass (measured as Chl-a). They attribute this increase in Chl-a to a greater influx of nutrients. The coupled biology/sea ice/ocean model used by Zhang et al. (2010) similarly showed that increased availability of both light and nutrients contributed to productivity increases for 1988–2007.

Spatial variation in nutrient supply, and thus phytoplankton productivity, is influenced by a variety of regional factors, such as ocean currents, stratification and mixing, and river inputs. High production in the southern Chukchi Sea is closely associated with a plume of nutrients that flows from the Pacific Ocean through Bering Strait (Lee et al., 2007; Tremblay et al., 2014). The Barents Sea, which is strongly influenced by

Atlantic inflow, also exhibits high production (Carmack et al., 2006; Randelhoff et al., 2015). Currents from both inputs spread into the interior Arctic Ocean (including the Beaufort, East Siberian, Laptev, and Kara Seas), but access to these water masses is impeded by strong stratification. In summer, sea ice melt generates a thin surface mixed layer that is cooler but substantially fresher than the Pacific and Atlantic waters below (Randelhoff et al., 2015, 2017; Steele et al., 2004). The water column is further stabilized as the fresh surface layer warms throughout summer (Randelhoff et al., 2017).

One mechanism that overcomes stratification and resupplies nutrients is upwelling along shelf breaks (Carmack et al., 2006; Carmack & Chapman, 2003; Tremblay et al., 2011). Because the Arctic Ocean shelves generally lie south of east-west shelf breaks, upwelling-favorable winds typically have an easterly component (Williams & Carmack, 2015). However, local bathymetry influences the strength of this relationship and dictates the most favorable wind direction (Williams & Carmack, 2008, 2015). For example, along the Canadian Beaufort Sea shelf, winds coming from 59° (the northeast) are most favorable for upwelling (Kirillov et al., 2016). Although most nitrogen in the southeast Beaufort Sea is recycled (Tremblay et al., 2008), upwelling of Pacific- and Atlantic-modified waters along the shelf break contributes new nutrients (Lin et al., 2019; Pickart et al., 2013; Tremblay et al., 2008, 2011). By supplying nutrients, sustained, strong, easterly winds along the Beaufort Sea shelf can enhance phytoplankton biomass (Mundy et al., 2009).

The shallow shelves of the interior seas are also influenced by rivers, especially near the mouths of the Mackenzie, Ob/Yenesei, Lena, and Kolyma Rivers (Carmack et al., 2006; Monier et al., 2014; Tank et al., 2011). However, the influence of rivers is complicated by competing factors. Rivers contribute additional nutrients (Le Fouest et al., 2013; Tremblay et al., 2014). However, rivers also increase turbidity, which reduces light availability (Hill, 2008), and they contribute freshwater at the surface, which reinforces stratification and inhibits access to deeper nutrients (Ardyna et al., 2014; Monier et al., 2014). Riverine impacts on overall Arctic productivity are minor, although they can be locally important near river mouths (Tank et al., 2011).

Recent studies indicate that another important mechanism is wind stress associated with summer Arctic storms, which may drive turbulent vertical mixing in the Arctic Ocean and lead to a temporary relief of phytoplankton nutrient limitation. Fer et al. (2017) observed enhanced mixing by storms during 2015. Oziel et al. (2017) observed higher Chl-a concentrations in the Barents Sea following a storm event in 2003. Nishino et al. (2015) and Uchimiya et al. (2016) found evidence that gale-force winds (>10 m s^{-1}) caused sufficient mixing to enhance phytoplankton productivity in the northern Chukchi Sea during a period in 2013 when the pycnocline was uplifted. Using a coupled biophysical model, Zhang et al. (2014) found that the Great Arctic Cyclone of August 2012 enhanced vertical mixing and phytoplankton productivity in the Chukchi, East Siberian, and Laptev Seas. These studies show that strong winds can induce enough turbulent vertical mixing to enhance nutrient availability and phytoplankton productivity, but the relative importance of wind stress likely varies by region and depends on the magnitude of the stress.

As Arctic sea ice continues to thin (Kwok, 2018) and the ice-free period continues to lengthen (Peng et al., 2018; Stroeve et al., 2016), further increases in NPP are possible, provided sufficient nutrients are available. Therefore, summer wind events may become more important to Arctic NPP in the future. A recent study by Ardyna et al. (2014) suggests that we may already be seeing a shift. In the past, most Arctic waters experienced a single plankton bloom in spring; however, Ardyna et al. (2014) observed that areas of the Arctic Ocean experiencing extended open-water periods sometimes exhibit a secondary plankton bloom in early fall. They attribute this secondary bloom to destabilization of the water column by surface winds, which now have more time to counteract stratification by sea ice melt and river discharge.

This study builds on this prior work to assess, on an aggregate basis, the hypothesis that high-wind events enhance seasonal productivity in the Arctic Ocean. We test this hypothesis by examining the statistical relationship between year-to-year variability in high-wind frequency and NPP during summer in the six marginal seas of the Arctic Ocean (labeled in Figure 1). We also control for other factors that may influence NPP during the study period: the amount of open water, sea surface temperature, and the direction of the zonal wind component. Although more nuance is apparent at a monthly time scale, we find strong evidence that stormier summers have higher NPP in the Barents and southern Chukchi Seas and some evidence for this relationship in the Laptev and East Siberian Seas.

2. Data

2.1. Net Primary Productivity (NPP)

NPP (g C m^{-2} day^{-1}) over the entire Arctic Ocean was determined from satellite derived Chl-a, SST, and sea ice cover (Arrigo & van Dijken, 2015). NPP is calculated hourly based on diel changes in light but uses a constant C:Chl ratio, a reasonable assumption for Arctic Ocean waters (Lewis et al., 2020). Chl-a was determined from satellite retrievals of remote sensing reflectance (R_{RS}) using the new Arctic Ocean-specific algorithm of Lewis and Arrigo (2020). This algorithm accounts for the unique bio-optical properties of Arctic waters that include greater pigment packaging (Huot et al., 2013; Matsuoka et al., 2007) and high concentrations of colored dissolved organic matter (Fichot et al., 2013; Matsuoka et al., 2007, 2011, 2017). SeaWiFS Level 3, 8-day $R_{RS}(\lambda)$ for years 1998–2007 (Reprocessing R2018.0) and MODIS Level 3 R_{RS} for years 2003–2018 (Reprocessing R2018.0) were acquired from the NASA Ocean Color website (https://oceancolor.gsfc.nasa.gov/). Because SeaWiFS Chl-a consistently exceeds MODIS Chl-a for the overlapping years of 2003–2007, a continuous time series was created by applying regional correction factors to all SeaWiFS Chl-a, as described in Lewis et al. (2020).

2.2. Open-Water and Ice-Free Periods

Daily sea ice concentration (SIC) on a 25 km by 25 km polar stereographic projection was obtained from the combined passive microwave record (Cavalieri et al., 1996; https://nsidc.org/data/NSIDC-0051/) for the period 1998–2019. These data were regridded to a 4 km by 4 km resolution to match the NPP data. Following the method of Stroeve et al. (2016), the "open-water period" at each grid cell is measured as the time between the last retreat day (the last time before the annual sea ice minimum that SIC falls below 75%) and first advance day (the first time after the annual sea ice minimum that SIC rises above 75%). Above that threshold, waters are considered ice-covered and NPP invalid. The "ice-free period" at each grid cell was also calculated based on a 10% threshold. The open-water period is used for NPP calculations; aggregates of each are used in the regression scheme described below.

2.3. Sea-Surface Temperature (SST) and Wind

Daily SST from the Reynolds Optimally Interpolated SST (OISST) Version 2.0 (Reynolds et al., 2007; https://www.ncdc.noaa.gov/oisst) was regridded to a 4 km by 4 km resolution. Near-surface (10-m) winds at a 0.75° latitude/longitude spatial resolution and 6-hr temporal resolution were obtained from the Interim European Reanalysis (ERA-I; Dee et al., 2011; https://apps.ecmwf.int/datasets/data/interim-full-daily/levtype=sfc/) for the period March 1998–February 2019. ERA-I wind estimates perform well in the Arctic when compared to those from other atmospheric reanalyses (Jakobson et al., 2012; Lindsay et al., 2014). Average wind speed, wind direction, and the frequency of high wind events are calculated from these data after regridding to a 4 km by 4 km polar stereographic projection. Following Ardyna et al. (2014) and Nishino et al. (2015), a high wind event is detected whenever the wind speed in a grid cell exceeds 10 m s^{-1} for one 6-hr observation.

3. Methods

3.1. Aggregation of Variables

For each year at each grid cell, the summer "study period" considered begins with either the first nonzero NPP observation or the beginning of the open-water period, whichever occurs later. Similarly, the study period ends with either the last nonzero NPP day or the end of the open-water period, whichever occurs first. The NPP product contains no data for any grid cell where ocean color cannot be detected because of cloud cover. Such gaps that fell within the study period were filled using the average NPP (gC m^{-2} day^{-1}) from the study period independently for each year and grid cell. Also, because NPP calculations are based on 8-day ocean color data, interpolation of NPP will only occur if there are at least two noncontiguous 8-day periods (at least 16 days total) of valid nonzero NPP observations. After interpolation, NPP is summed to obtain total NPP (gC m^{-2}) for the study period. SST was averaged for the entire study period at each grid cell. The percentage of 6-hr observations in the study period for which (a) winds exceed 10 m s^{-1} and (b) the zonal wind component was westerly was also recorded. This accounts both for the frequency of high-wind events and the general direction of winds in each period (e.g., whether wind direction favors upwelling along the shelf breaks). Temporal summation/averaging for individual months was conducted in a similar fashion, but the

monthly period for each year and grid cell was taken as the intersection of days in that month and days in the respective seasonal study period.

Next, regionalization of SST and wind variables was conducted using temporal and spatial weighting (see Figure 1 for regions). A grid cell is weighted both by its area and by the length of its study period for each year. The product of temporally integrated NPP (gC m^{-2}) and grid cell area (m^2) is summed for all grid cells in the region to yield a total seasonal NPP (gC). The ice-free period (continuous days when sea ice concentration is below 10%) for each grid cell was summed, yielding "ice-free observations" (days * grid cells). The number of ice-free observations in a region for a given period increases if (a) a given grid cell is ice-free for more days during the summer or (b) on a given day, more grid cells are ice-free. "Open water observations" were calculated as the area-weighted summation of 1—SIC for all grid cells within the study period (where SIC ≤75%). In other words, open-water observations (OWOs) are a temporal integration of open water area during the study period, and ice-free observations (IFOs) are a temporal integration of a binary (1 = ice-free, 0 = ice present) independent of study period. This is roughly analogous to integrating the inverse of sea ice area and sea ice extent, respectively.

Regionalization is used rather than working by grid cell in part because of the different projections and spatial resolutions of the input data. More importantly, the spatial scale of the relationship being tested is likely regional. Wind stress occurring over a single grid cell of the ocean will impact more than the column of water directly below that area. For example, phytoplankton cells can be advected over many horizontal grid cells over the course of a month or season. Regionalization reduces the impact of these issues.

However, aggregation has its own complications. The length of the ice-free period varies from year to year for each grid cell, as does the number of ice-free grid cells in a region for any given period. With both dimensions being inconstant, we adopted the variables "ice-free observations" and "open water observations" to encapsulate both spatial and temporal changes. The benefit of this approach is that the consolidation of two related concepts (e.g., longer ice-free period and larger ice-free area) into a single variable is flexible and efficient. Additionally, it allows us to assess whether any perceived relationship between SST or wind variables and NPP exists because both variables are related the amount of open water (see section 3.2).

3.2. Multiple Linear Regression

The research question for this study is whether, after controlling for variability in the amount of open water and SST in a region of the Arctic Ocean, the frequency of high-wind events throughout a month or year has a measurable impact on NPP. Therefore, a multiple linear regression model with four x-variables was constructed for seven regions of the Arctic Ocean for the extended summer season (May–September). Models were also constructed for every month June through September, except for the East Siberian Sea, which only has a sufficient number of NPP observations in July through September. Each model follows the form:

$$NPP = \alpha + \beta_1 IFO + \beta_2 SST + \beta_3 HWF + \beta_4 WWF \quad (1)$$

where IFO is the number of IFOs, high-wind frequency (HWF) is the percentage of wind observations that exceed 10 m s^{-1}, and westerly wind frequency (WWF) is the percentage of wind observations with a westerly component (i.e., from the west). All variables were converted to *Z*-scores before insertion into the models to standardize units. While we focus on NPP here, we note that the impact of high winds on NPP is closely related to the impact of high winds on phytoplankton biomass, as indicated by correlations with chlorophyll *a* concentration (supporting information Tables S1 and S2); this is consistent with the study by Lewis et al. (2020).

Ordinary least squares regression models were constructed using every possible combination of those four x-variables, and the model with the lowest the Bayesian information criterion (BIC) is reported in section 4. Lower BIC indicates better model performance based on a maximum likelihood function and the number of observations and x-variables (Schwarz, 1978). Using fewer x-variables yields a lower BIC, favoring a parsimonious model.

Especially with temporal aggregation, the amount of open water can be measured in several ways, so the entire regression scheme was repeated replacing IFOs with OWOs:

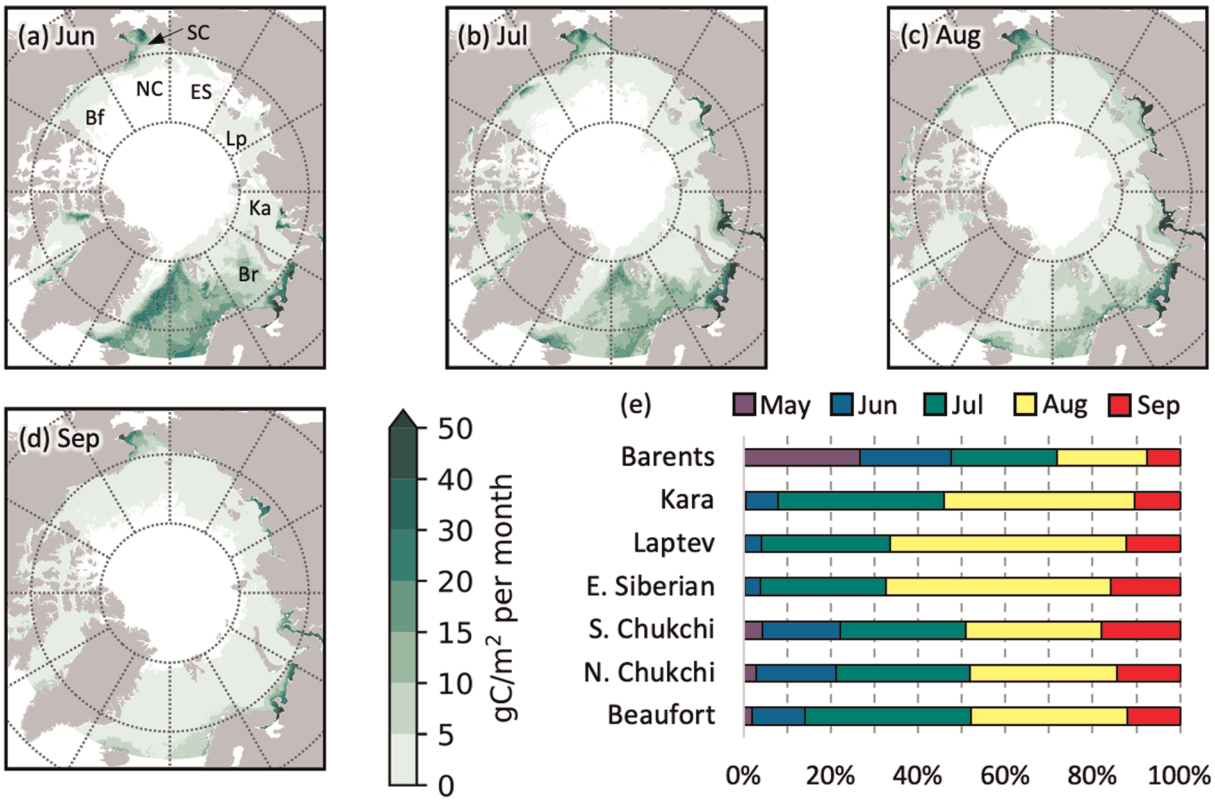

Figure 2. (a–d) Maps of average monthly NPP (1998–2018) for grid cells with at least 1 year of nonzero NPP observations. (e) Average percentage of total summer NPP that occurs in each month by region.

$$NPP = \alpha + \beta_1 OWO + \beta_2 SST + \beta_3 HWF + \beta_4 WWF \quad (2)$$

We show results with 75% SIC as the open-water threshold, but using 50% SIC as the open-water threshold yields similar results. Using OWOs provides a more direct match to the time and area over which NPP is aggregated than using IFOs. However, high SIC areas often have a positive open water bias due to misidentification of melt ponds as open water (Ivanova et al., 2015; Rosel et al., 2012), so IFOs are likely a more robust measure.

Additionally, as the amount of open water increases, the ocean warms, which means that SST is positively correlated with both IFO and OWO. In 30 of the 34 region/period combinations assessed with regression models, that correlation is significant for SST and OWO. For OWO and NPP, the count jumps to 32 of 34. This relationship is the root of multicollinearity in several of the models constructed using Equations 1 and 2. Variance inflation factors (VIFs) are between 2.0 and 3.0 for IFO and SST in several models for which both variables are present (Tables S3 and S4). This indicates minor inflation of R^2 and the respective variables' coefficients (Chatterjee & Simonoff, 2013). Multicollinearity is a bigger problem in the models using OWO, with the highest VIF exceeding 5.0 (Tables S5 and S6). However, in no case does any wind variable have a VIF above 2.0, indicating that the wind variables are not notably biased by changing amounts of open-water each year.

4. Results and Discussion

4.1. Monthly Regional Climatologies

Understanding the spatial variation in the monthly climatology of each input variable is necessary to accurately interpret the results of the regression process described above. For example, most regions experience a large majority of summer NPP during the months of July and August (Figure 2e), with the most widespread productivity occurring in August (Figure 2c). June and September contribute smaller percentages, and only

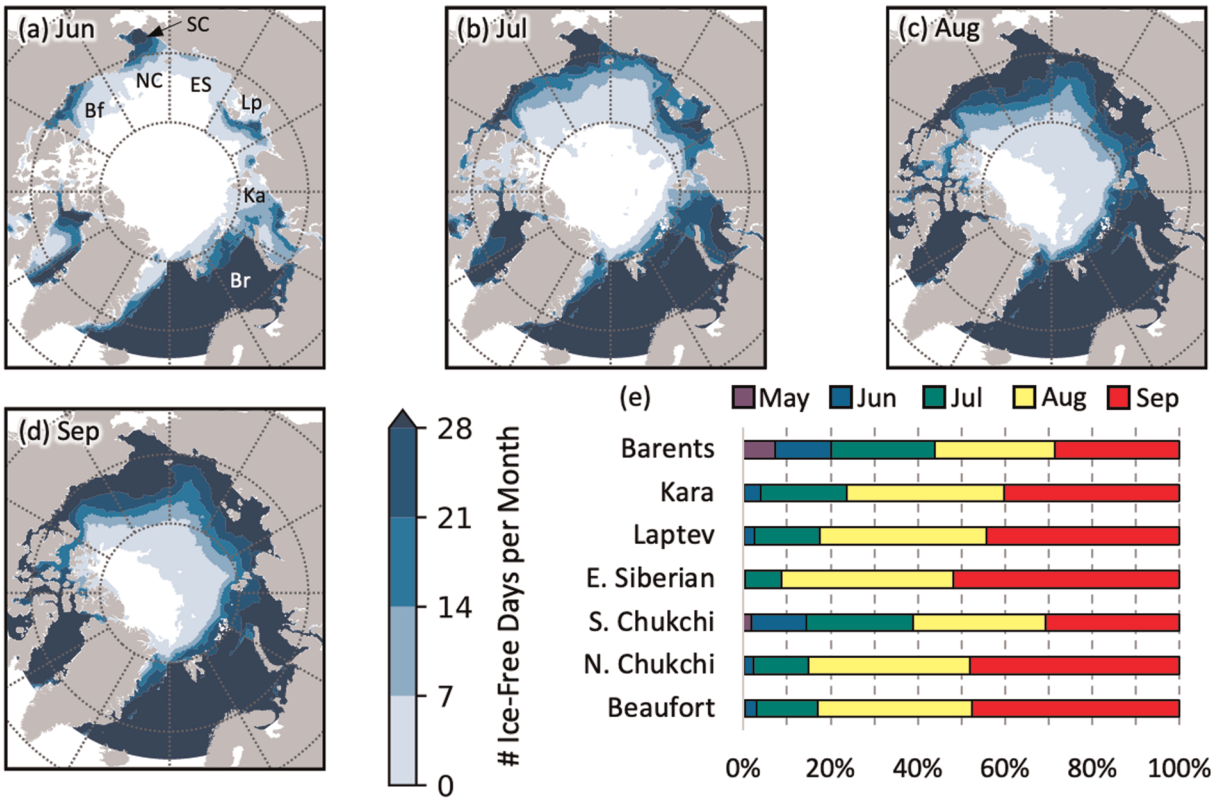

Figure 3. (a–d) Maps of average number of ice-free days (1998–2018). An average of exactly zero days is colored white. (e) Average percentage of total summer ice-free days occurring each month by region.

the Barents Sea experiences more than 5% of its summer NPP in May. Additionally, although some NPP occurs in June in other regions, only the Barents and southern Chukchi Seas experience substantial productivity in that month (Figure 2a). The lower NPP in September is partly due to lower productivity rates (fewer gC m^{-2} day^{-1}) (Figure S1) but also because the scan area for both SeaWiFS and MODIS shifts south in the fall, so recorded NPP falls to 0 gC m^{-2} day^{-1} during September for most Arctic Ocean grid cells even though some productivity persists (Figure S2).

Much of this seasonal pattern can be explained by the number of ice-free days in each month (Figures 3a–3d). Sea ice retreats earliest in the Barents and southern Chukchi Seas, and the southwestern part of the Barents Sea is ice-free year-round. These inflow seas of the Arctic Ocean are heavily influenced by northward oceanic heat fluxes: through the Bering Strait to the southern Chukchi Sea (Serreze et al., 2016, 2019; Woodgate, 2018) and via the North Atlantic Ocean to the Barents Sea (Årthun et al., 2012; Smedsrud et al., 2013; Timmermans & Marshall, 2020). The shelves of the other seas experience sea ice retreat primarily in July (Figure 3b), and water is mostly ice-free throughout August and September for all the shelves (Figures 3c and 3d). However, because satellite retrievals for high latitudes cease partway through September, not all IFOs from the passive microwave record have a corresponding NPP observation (Figure S2d). Therefore, the study period for many grid cells ends before the end of the ice-free period.

The pattern of opening observed with ice-free days is closely followed by the seasonal increase in SST from June through August (Figure 4). The Barents, Kara, Laptev, and East Siberian Seas are warmest in September, but the Chukchi and Beaufort Seas are slightly warmer in August. Ice-free waters in the Laptev, Kara, and Barents Sea extend farther north than in other seas during August (Figure 3c). When these seas experience a reduction in grid cells with valid data in September (Figure 3i), that reduction comes from generally cooler grid cells, so the average SST increases for September.

Wind is measured in two ways for this study. First, the percentage of time during the study period for which wind speed exceeds 10 m s^{-1} is the high-wind frequency (HWF; Figure 5). The Barents Sea, at the end of the

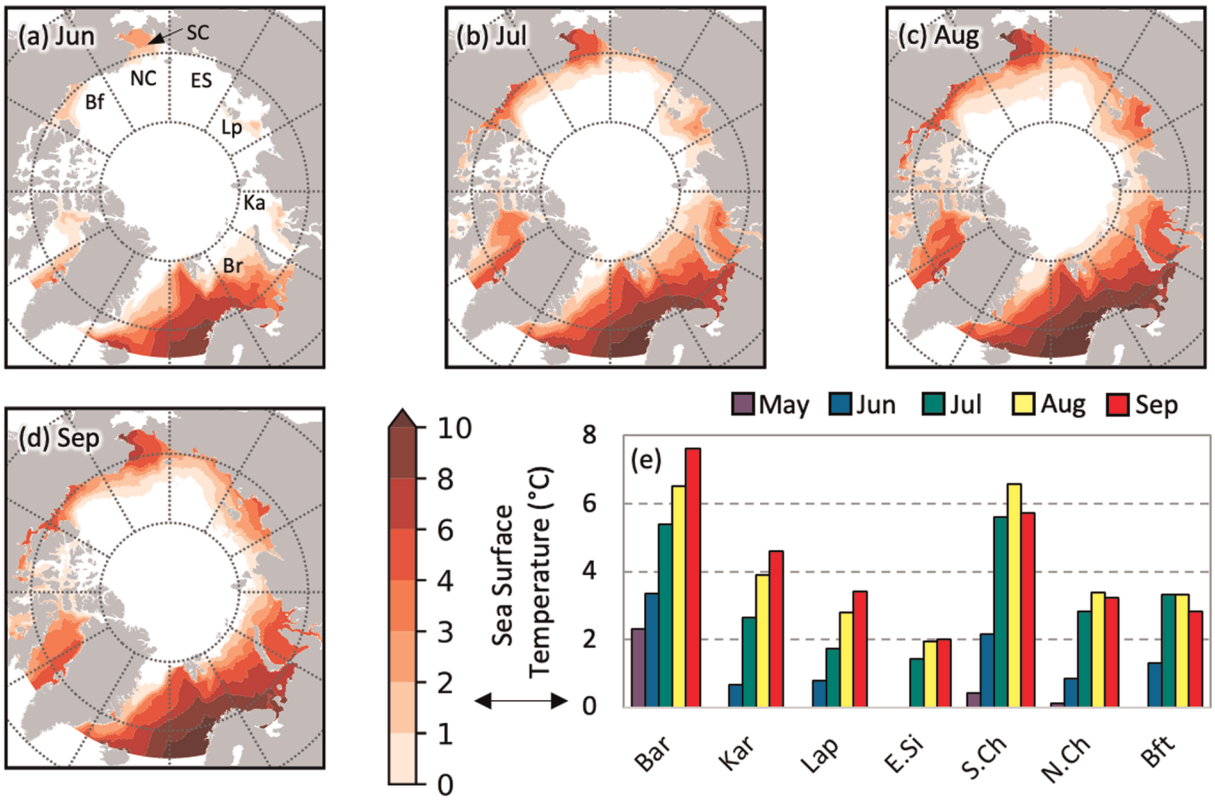

Figure 4. (a–d) Maps of average sea-surface temperature. Averages for each grid cell are restricted to years in the period 1998–2018 that have nonzero NPP and open water. (e) Average sea-surface temperature during study period by region.

North Atlantic storm track (Rogers, 1997; Serreze et al., 1997), has the greatest frequency of high winds in both June and September. However, high-wind frequency is similar in the Kara, Laptev, and Chukchi Seas during July and August, when the Arctic storm track is at its peak strength (Crawford & Serreze, 2016; Tilinina et al., 2014). In July and August, high-wind events are least frequent in the Beaufort Sea (Figure 5e).

Second, westerly wind frequency (WWF) is the percentage of time during the study period for which the zonal wind component is westerly (Figure 6). The Beaufort Sea High (Serreze & Barrett, 2011) is a dominant feature on the Pacific side of the Arctic Ocean. Clockwise circulation around this high means predominantly easterly winds in the Beaufort Sea, northern Chukchi Sea and, to a lesser extent, the East Siberian Sea. Other seas experience variable wind direction throughout summer, although westerly winds are more common than easterly winds in the Barents, Kara, and Laptev Seas in September. Note that for Figures 5 and 6, especially high percentages sometimes appear on the northern fringes of the valid area because of conditions particular to the years with the smallest sea ice extent (especially 2007, 2012, and 2016). Although apparently strong, they have only a small impact on regional averaging because the average ice-free period is short for those grid cells.

4.2. Regression Models for Annual NPP Using Ice-Free Observations

Regression models for annual NPP demonstrate that, for several regions of the Arctic Ocean, greater frequency of high-wind events is associated with greater NPP (Table 1). Each model reported has the lowest possible BIC for that region for any combination of the four variables. Since BIC increases with each additional x-variable, an x-variable is only present in the lowest-BIC model if it substantially improves model fit. The inclusion of high-wind frequency (HWF) in four of seven regions shows that knowing the HWF improves prediction of NPP for those seas. For all regions that include HWF in the regression model, the coefficient for HWF is positive and significant at $p < 0.10$.

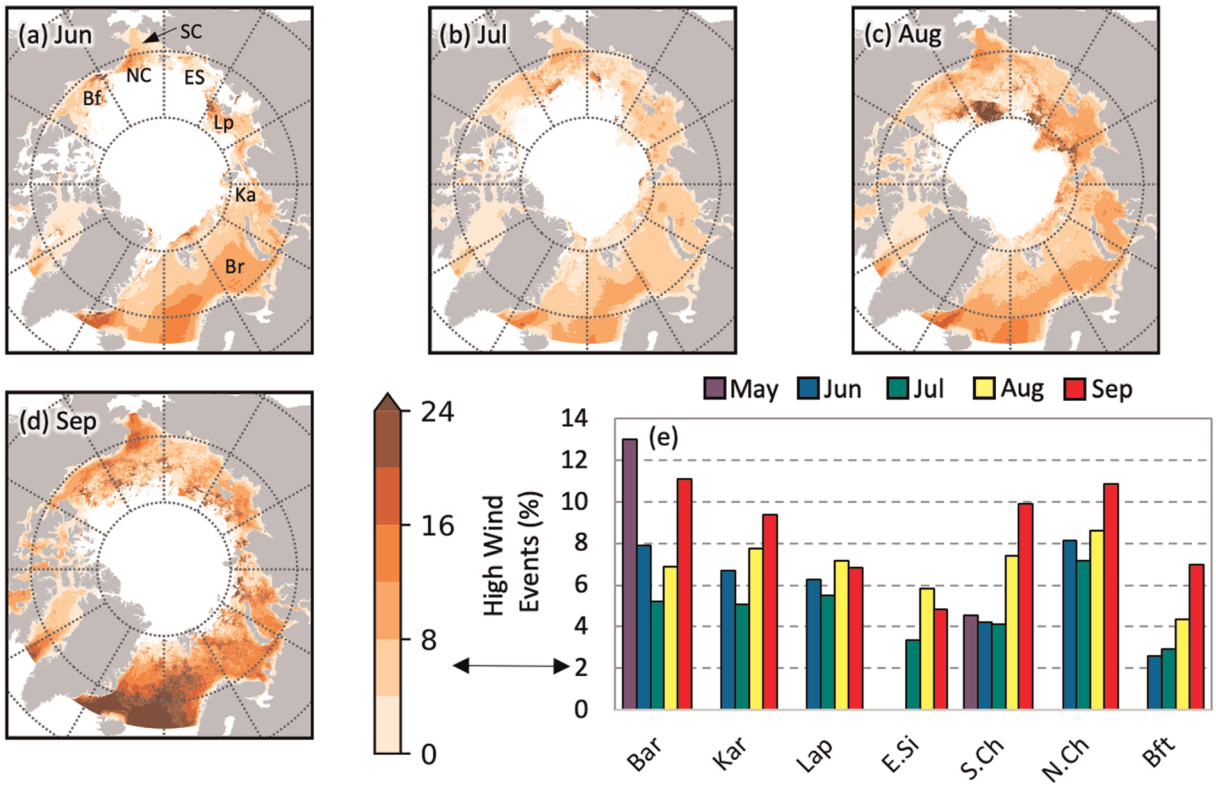

Figure 5. As in Figure 4, but for high-wind frequency.

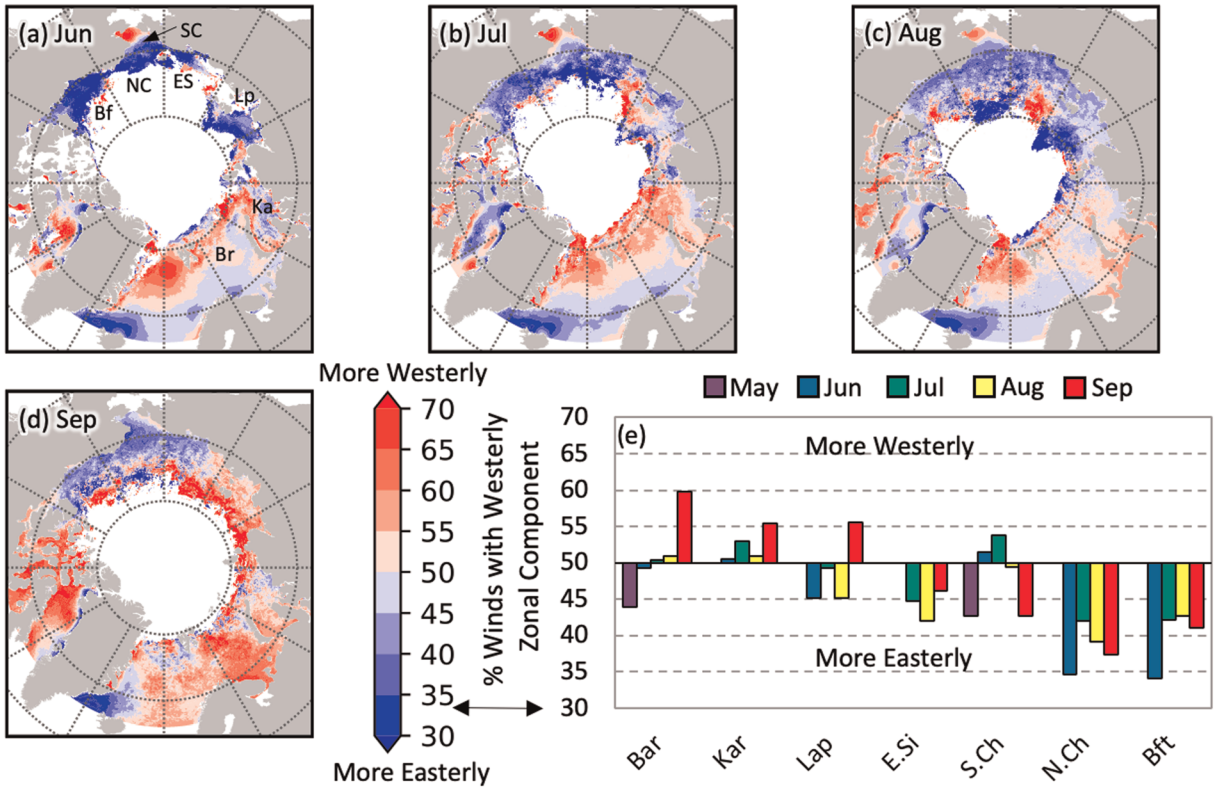

Figure 6. As in Figure 4, but for westerly wind frequency. Note that a percentage over 50% (red in maps) means that westerly winds are more common and a percentage below 50% (blue) means that easterly winds are more common.

Table 1
Results of Multiple Linear Regression Models With the Lowest BIC Values Using Equation 1 to Describe Seasonal NPP

Region	R^2	IFO	SST	HWF	WWF
Barents	0.55	—	**0.54**	*0.31*	*0.29*
Kara	0.84	**0.78**	*0.24*	—	*−0.19*
Laptev	0.88	**0.48**	**0.49**	*0.17*	—
E. Siberian	0.91	**0.42**	**0.60**	**0.18**	—
S. Chukchi	0.61	**0.61**	**0.41**	*0.32*	—
N. Chukchi	0.76	**0.72**	*0.24*	—	—
Beaufort	0.82	**0.77**	—	—	**−0.38**

Note. Bold and italic text indicate $p < 0.05$ and $p < 0.10$, respectively. All coefficients have standardized units.

Previous studies demonstrate that high-wind events, such as those associated with the passage of strong synoptic-scale cyclones, can lead to increases in NPP (e.g., Nishino et al., 2015; Oziel et al., 2017; Zhang et al., 2014). However, it is sometimes unclear how much of the observed increases in NPP in a particular area following storms reflects a redistribution of NPP versus an overall increase, such as in the August 2012 case examined by Zhang et al. (2014). The results from these regression models show that the impacts of high-wind events are not restricted to localized areas for short periods; they can have large-scale impacts on seasonal-scale NPP in the Arctic Ocean. After controlling for the amount of ice-free days and SST, a stormier summer is generally a more productive summer for the Barents, Laptev, East Siberian, and southern Chukchi Seas.

Moreover, an increase in HWF from 1998 to 2018 may explain some of the simultaneous increase in NPP (Tables S7 and S8; Arrigo & van Dijken, 2015; Bélanger et al., 2013; Lewis et al., 2020). Although much of the increase in NPP can be attributed to an increase in open water (Arrigo & van Dijken, 2015; Bélanger et al., 2013; Lewis et al., 2020), significant positive trends in HWF from 1998 to 2018 in the Barents, Kara, and East Siberian Seas (Figure 7) suggest that increased storminess may be another contributing factor. Although not significant, trends in the other regions are also all positive for that period. This finding is consistent with those of Ardyna et al. (2014), although their data were for September and October, whereas the study period here may start anytime from May to July and ends sometime in September (depending on the year and location). An increase in deep/extreme Arctic storms has also been found in some cyclone studies (e.g., Sepp & Jaagus, 2010; Vavrus, 2013), although not in others (e.g., Zahn et al., 2018).

The importance of high-wind events should not be overstated, though. Note that HWF is never the primary factor controlling NPP. Because all data were standardized (converted to *Z*-scores) before model construction, the magnitude of the coefficients reflects the relative importance of each x-variable in predicting variability in NPP. For all seas, the number of IFOs or SST has the largest coefficient.

Two of the regions for which HWF does not help explain the interannual variability in NPP are the Beaufort and northern Chukchi Seas. These regions are the most strongly impacted by the Beaufort Sea High. Most Beaufort Sea IFOs are restricted to the narrow shelf along the Beaufort coast in this study, and the easterly winds associated with the Beaufort Sea High are generally favorable for upwelling along the shallow shelf break (Kirillov et al., 2016; Meneghello et al., 2018; Randelhoff & Sundfjord, 2018). Such upwelling is a major source of nutrients (Kirillov et al., 2016; Mundy et al., 2009; Schulze & Pickart, 2012; Tremblay et al., 2011). In other words, wind direction may be more important in the Beaufort Sea than in other regions because wind inducing shelf-break upwelling is more essential to nutrient replenishment than wind breaking down the pycnocline.

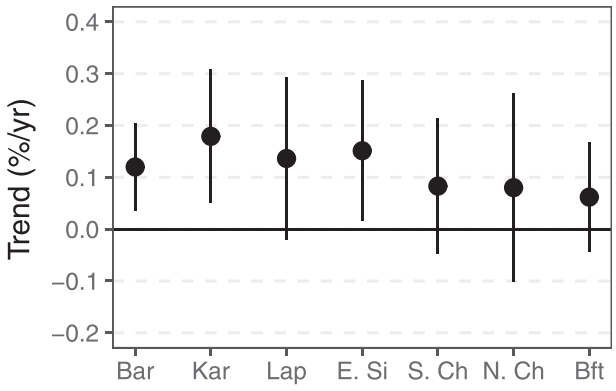

Figure 7. Linear trends (1998–2018) in high-wind frequency (% year^{-1}) during the study period by region, along with 90% confidence interval.

Another region for which westerly wind frequency is included in the regression model is the Barents Sea, for which more frequent westerly winds are associated with higher NPP. This statistical model might be capturing in part the relationship between local winds and Atlantic inflow to the Barents Sea. A stronger North Atlantic storm track (i.e., positive North Atlantic Oscillation) tends to increase Atlantic inflow (Lien et al., 2017), and Atlantic waters are relatively nutrient-rich (Oziel et al., 2017; Randelhoff et al., 2016).

4.3. Regression Models for Annual NPP Using Open-Water Observations

To test the sensitivity of these results to how open water is measured, the regression model scheme was repeated using OWOs (Equation 2; Table 2) instead of IFOs (Equation 1; Table 1). Recall that OWO is an integration of open-water area, whereas IFO is an integration of the inverse of sea-ice extent. Results from Equation 2 suggest that

Table 2
Results of Multiple Linear Regression Models With the Lowest BIC Values Using Equation 2 to Describe Seasonal NPP

Region	R^2	OWO	SST	HWF	WWF
Barents	0.77	**0.62**	**0.34**	*0.21*	—
Kara	0.84	**0.92**	—	—	—
Laptev	0.87	**0.61**	**0.40**	—	—
E. Siberian	0.97	**0.78**	**0.24**	—	—
S. Chukchi	0.82	**0.81**	**0.27**	**0.28**	—
N. Chukchi	0.90	**0.95**	—	—	—
Beaufort	0.93	**0.72**	**0.34**	—	—

Note. Bold and italic text indicate $p < 0.05$ and $p < 0.10$, respectively. All coefficients have standardized units.

variability in OWO is better than variability in IFO at predicting NPP. The R^2 values are generally higher, and OWO always has the highest coefficient in Equation 2 models.

Additionally, with OWO being a stronger explanatory variable, the secondary factors become less able to improve model fit. Westerly wind frequency is excluded from all lowest-BIC models, and high-wind frequency only appears in the models for two regions rather than four. (If included, the coefficients for HWF in the Laptev and East Siberian Sea models would still be positive, but not significant.) This indicates that a positive relationship between high-wind frequency and NPP is only robust in the Barents and southern Chukchi Seas, which may result in part because high winds blowing over these seas can more reliably access nutrients supplied by inflow from the Atlantic Ocean (Oziel et al., 2017; Randelhoff et al., 2016) or through Bering Strait (Lee et al., 2007; Tremblay et al., 2014). The Laptev and East Siberian Seas, on the other hand, are both interior shelves. Additionally, these two regions have the longest ice-free periods, and variability in OWOs is low (Figure 3).

4.4. Regression Models for Monthly NPP

Breaking down these variables by month (Table 3) shows that different variables are more important during different parts of the study period. The number of ice-free days is essential in earlier months, when sea ice is rapidly retreating throughout most of the Arctic Ocean. This is similar to findings by Kahru et al. (2016), who found open-water variability in June has a greater impact on annual NPP than open-water variability in other months. In the Barents, Kara, and southern Chukchi Seas, where sea ice retreats earliest, the number of IFOs is only important to NPP in June. The Barents Sea, most of which is open year-round, is the only sea for which the number of IFOs is not important on a seasonal timescale. Conversely, SST is the dominant factor by September in all regions except the East Siberian Sea, which is the last region to open up.

Using OWOs instead of IFOs yields less variation by month (Table 4). OWO is the dominant x-variable in almost every month-region combination. SST is still less relevant in June than other months, but it does not become the dominant factor in August and September. In September, this result is somewhat artificial: The last OWO in a grid cell may occur from either the return of sea ice or the ocean color sensors shifting their view to more southerly latitudes. A cloudy period at the end of satellite viewing may cut off the study

Table 3
Results of Multiple Linear Regression Models With the Lowest BIC Values Using Equation 1 to Describe Monthly NPP

	June					July				
Region	R^2	IFO	SST	HWF	WWF	R^2	IFO	SST	HWF	WWF
Barents	0.60	—	**0.50**	**0.49**	—	0.33	—	**0.57**	—	—
Kara	0.91	**0.95**	—	—	—	0.81	—	**0.90**	—	—
Laptev	0.87	**0.91**	—	**0.28**	—	0.89	**0.85**	—	**0.29**	—
E. Siberian	—	—	—	—	—	0.90	**0.95**	—	—	—
S. Chukchi	0.71	**0.84**	—	—	—	0.30	—	**0.55**	—	—
N. Chukchi	0.80	**0.47**	*0.26*	*0.27*	*−0.22*	0.94	**0.94**	—	—	**−0.13**
Beaufort	0.71	—	**0.73**	**0.30**	—	0.89	**0.49**	**0.38**	**0.24**	**−0.21**
	August					September				
Region	R^2	IFO	SST	HWF	WWF	R^2	IFO	SST	HWF	WWF
Barents	0.50	—	**0.71**	—	—	0.69	—	**0.83**	—	—
Kara	0.52	—	**0.72**	—	—	0.43	—	**0.66**	—	—
Laptev	0.73	**0.39**	**0.58**	—	—	0.38	—	**0.62**	—	—
E. Siberian	0.77	**0.46**	**0.49**	—	—	0.31	**0.56**	—	—	—
S. Chukchi	0.45	—	**0.67**	—	—	0.41	—	**0.64**	—	—
N. Chukchi	0.66	**0.60**	**0.33**	—	—	0.46	—	**0.68**	—	—
Beaufort	0.78	**0.52**	*0.28*	**−0.29**	**−0.52**	0.09	—	—	—	−0.29

Note. Bold and italic text indicate $p < 0.05$ and $p < 0.10$, respectively. All coefficients have standardized units.

Table 4
Results of Multiple Linear Regression Models With the Lowest BIC Values Using Equation 2 to Describe Monthly NPP

	June					July				
Region	R^2	OWO	SST	HWF	WWF	R^2	OWO	SST	HWF	WWF
Barents	0.73	**0.86**	—	—	—	0.56	**0.51**	**0.38**	—	—
Kara	0.96	**0.90**	0.11	—	—	0.81	**0.54**	**0.41**	—	—
Laptev	0.93	**0.97**	—	—	—	0.87	**0.87**	—	**0.23**	—
E. Siberian	—	—	—	—	—	0.95	**0.72**	**0.27**	—	—
S. Chukchi	0.86	**0.71**	*0.27*	—	—	0.60	**0.55**	**0.43**	*0.29*	—
N. Chukchi	0.93	**0.91**	—	*0.12*	—	0.95	**0.82**	**0.17**	—	**−0.12**
Beaufort	0.93	**0.73**	**0.22**	—	**−0.19**	0.83	**0.67**	*0.29*	—	—
	August					September				
Region	R^2	OWO	SST	HWF	WWF	R^2	OWO	SST	HWF	WWF
Barents	0.50	—	**0.70**	—	—	0.84	**0.51**	**0.50**	—	—
Kara	0.56	**0.75**	—	—	—	0.80	**0.89**	—	**−0.30**	—
Laptev	0.76	**0.49**	**0.49**	—	—	0.86	**0.72**	**0.35**	—	*0.18*
E. Siberian	0.87	**0.93**	—	—	—	0.91	**0.95**	—	—	0.12
S. Chukchi	0.65	**0.50**	**0.46**	*0.30*	—	0.53	**0.37**	**0.48**	—	—
N. Chukchi	0.88	**0.94**	—	—	—	0.82	**0.73**	*0.26*	—	—
Beaufort	0.73	**0.49**	*0.32*	—	**−0.37**	0.34	**0.59**	—	—	—

Note. Bold and italic text indicate $p < 0.05$ and $p < 0.10$, respectively. All coefficients have standardized units.

period prematurely (because ocean color cannot be retrieved). Especially for the Barents Sea, most of which is ice-free all month (Figure 3d), this leads to greater variability in OWO than IFO in September. Therefore, the importance of OWO to NPP in September is likely overestimated.

As with the seasonal models, monthly models show a stronger connection between high winds and NPP if IFO (Equation 1; Table 3) are used instead of OWOs (Equation 2; Table 4). Wind variables are still present (and significant) in several models using Equation 2; however, they are not necessarily the same months and regions as in the models based on Equation 1. Therefore, it is only appropriate to interpret general patterns and the few instances for which results are insensitive to regression scheme.

Two consistent results for high-wind frequency are notable in Tables 3 and 4. First, NPP is higher in the Laptev Sea in July when high winds are more common. Second, HWF with a positive significant coefficient is included in the lowest-BIC model for several models in June and July, one in August, and none in September. Therefore, high-wind frequency appears more important to early-season growth. These results contrast with those of Ardyna et al. (2014), who, when comparing the number of stormy days to the occurrence of fall blooms in Arctic waters, highlighted the importance high-wind events during September and October. The NPP model used here calculates no NPP by mid-September in a large percentage of grid cells with open water. We still find a significant role for high-wind events affecting NPP, but we do not find the relationship to be prominent in September.

The Beaufort and northern Chukchi Seas both show some months with a significant role for westerly-wind frequency. Again, the relationship is more prominent using IFOs rather than OWOs. The coefficient is consistently negative for westerly wind frequency in these two regions, indicating that a higher frequency of easterly winds is associated with more NPP. As with the seasonal results, this indicates that wind direction is more important to nutrient availability than wind speed because easterly winds are favorable for upwelling along the shelf break of Beaufort and northern Chukchi Seas (Kirillov et al., 2016; Lin et al., 2019; Schulze & Pickart, 2012). This may be in part because, whereas wind direction has an easterly zonal component in about two thirds of Beaufort Sea wind observations, high-wind observations occur about equally often with an easterly or westerly zonal component. (The passage of cyclones disrupts the normal, upwelling-favorable, anti-cyclonic circulation.)

4.5. Limits to Experimental Design

One major limit to this study is the inability of satellite sensors to detect all NPP in the Arctic Ocean. Chlorophyll *a* measurements are impeded by sea ice cover, so sub-ice phytoplankton growth is not

captured (Arrigo & van Dijken, 2015). Satellite sensors also have difficulty detecting subsurface chlorophyll maxima (Ardyna et al., 2013; Arrigo & van Dijken, 2011). Especially early in the growth season, the limited area of NPP observations makes the influence of chromophoric dissolved organic matter (CDOM) supplied by rivers a major concern. CDOM can lead to a positive bias in chlorophyll *a* measurements (Lewis et al., 2016; Vetrov et al., 2008). These issues can be resolved by specifically tuning a productivity model to the distinct conditions of the various regions of the Arctic Ocean (IOCCG, 2015; Lee et al., 2015). For example, the productivity model used here is tuned to in situ observations from cruises throughout the Arctic Ocean (Lewis & Arrigo, 2020), and the algorithm used here has performed well in comparison to in situ observations (Arrigo & van Dijken, 2011; Lewis & Arrigo, 2020). Cloud cover also hinders chlorophyll *a* retrievals, making complete Arctic-wide daily NPP observations impossible. Therefore, although wind values are available at a subdaily temporal resolution from ERA-I, the NPP data are insufficient for a storm-by-storm analysis. Although sacrificing resolution, spatial and temporal aggregation leads to more robust results.

However, recall that aggregation means variable amounts of open water year to year and bias in models due to the correlation between SST and OWOs/IFOs. Because this issue was greater for SST and OWOs, higher R^2 values reported for several models in Tables 2 and 4 (compared to Tables 1 and 3) are inflated and may not represent a better fit. Thus, the regression scheme yields more reliable results when using IFOs from a statistical standpoint even though using OWOs is a more logical variable from a physical standpoint.

With finer resolution, the impact of individual events could be explored systematically. Such detailed analysis would better distinguish between the relative importance of (a) high wind speeds reducing stratification versus (b) upwelling-favorable wind direction on nutrient availability in smaller regions. Another way to add detail would be including a more precise measure of upwelling-favorable wind direction for each locality. Including southerly wind frequency (Figure S3) in the regression scheme makes little difference to seasonal results, although southerly wind fraction appears in several September models (Tables S9 and S10). We also did not attempt to disentangle the effects of high-wind events from increased cloudiness, both of which are associated with synoptic-scale cyclones. Cloudier conditions reduce light availability and can reduce NPP (Bélanger et al., 2013). Therefore, significant relationships between high-wind frequency and NPP were found despite that counteracting relationship.

5. Conclusions

The purpose of this paper was to evaluate the hypothesis that Arctic Ocean NPP is enhanced by high-wind events, which increase vertical mixing in the Arctic Ocean, stirring up more nutrients, and thereby enhancing NPP. This was accomplished by including high-wind frequency as an x-variable in linear regression models of regional NPP while controlling for the amount of open water, the SST, and zonal wind direction. For each combination of region and time period, the lowest-BIC model of all models with any combination of the possible x-variables was identified as the best fit. The hypothesis that NPP is enhanced by high-wind events was supported wherever high-wind frequency was a significant x-variable with a positive coefficient in that lowest-BIC model. Based on these criteria, four regions of the Arctic Ocean show some tendency for greater high-wind frequency increasing NPP. However, this relationship is only robust at the seasonal timescale for the two inflow seas (the Barents and southern Chukchi Seas). We also find stronger evidence for high-wind frequency influencing NPP earlier in summer (June and July). Finally, an easterly wind direction is more important than high wind speed to enhancing NPP in the Beaufort and northern Chukchi Seas.

The results shown here for the Barents Sea are particularly notable. Lewis et al. (2020) found significant increases to NPP in the Barents Sea despite no simultaneous increase in open-water duration. Therefore, increased NPP likely comes from greater nutrient availability, but prebloom concentrations of silicate (Hátún et al., 2017; Rey, 2012) and nitrate (Oziel et al., 2017) in Atlantic waters have decreased in recent years. Our results show that (a) summer NPP in the Barents Sea is significantly higher during summers with greater high-wind frequency (Tables 1 and 2) and (b) that high-wind events are becoming increasingly common in the Barents Sea (Figure 7). This suggests that increased high-wind frequency is behind the enhanced NPP in the Barents Sea reported by Lewis et al. (2020).

Data Availability Statement

Bio-optical data used to develop the Arctic Chl-a algorithm as well as time series data for Chl-a, NPP, and SST are available on the Dryad data repository (http://doi.org/10.5061/dryad.cnp5hqc17). Code used for aggregation and statistical analysis are stored on Zenodo (https://doi.org/10.5281/zenodo.3985150).

Acknowledgments
N. S. L. and K. M. K. are grateful for funding from the National Science Foundation (OCE-1752724 and OCE-1558225). This material is based upon work supported by the National Center for Atmospheric Research, which is a major facility sponsored by the National Science Foundation under Cooperative Agreement No. 1852977.

References

Ardyna, M., Babin, M., Gosselin, M., Devred, E., Bélanger, S., Matsuoka, A., & Tremblay, J.-É. (2013). Parameterization of vertical chlorophyll a in the Arctic Ocean: Impact of the subsurface chlorophyll maximum on regional, seasonal, and annual primary production estimates. *Biogeosciences*, *10*(6), 4383–4404. http://doi.org/10.5194/bg-10-4383-2013

Ardyna, M., Babin, M., Gosselin, M., Devred, E., Rainville, L., & Tremblay, J.-E. (2014). Recent Arctic Ocean sea ice loss triggers novel fall phytoplankton blooms. *Geophysical Research Letters*, *41*, 6207–6212. http://doi.org/10.1002/2014GL061047

Arrigo, K. R., Perovich, D. K., Pickart, R. S., Brown, Z. W., van Dijken, G. L., Lowry, K. E., et al. (2012). Massive phytoplankton blooms under Arctic Sea ice. *Science*, *336*(6087), 1408–1408. http://doi.org/10.1126/science.1215065

Arrigo, K. R., Perovich, D. K., Pickart, R. S., Brown, Z. W., van Dijken, G. L., Lowry, K. E., et al. (2014). Phytoplankton blooms beneath the sea ice in the Chukchi Sea. *Deep Sea Research Part II: Topical Studies in Oceanography*, *105*, 1–16. http://doi.org/10.1016/j.dsr2.2014.03.018

Arrigo, K. R., van Dijken, G., & Pabi, S. (2008). Impact of a shrinking Arctic ice cover on marine primary production. *Geophysical Research Letters*, *35*, 529. http://doi.org/10.1002/9780470757161.ch5

Arrigo, K. R., & van Dijken, G. L. (2011). Secular trends in Arctic Ocean net primary production. *Journal of Geophysical Research*, *19*, L19603. http://doi.org/10.1175/JCLI3767.1

Arrigo, K. R., & van Dijken, G. L. (2015). Continued increases in Arctic Ocean primary production. *Progress in Oceanography*, *136*, 60–70. https://doi.org/10.1016/j.pocean.2015.05.002

Årthun, M., Eldevik, T., Smedsrud, L. H., Skagseth, Ø., & Ingvaldsen, R. B. (2012). Quantifying the influence of Atlantic heat on Barents Sea ice variability and retreat. *Journal of Climate*, *25*(13), 4736–4743. http://doi.org/10.1175/JCLI-D-11-00466.1

Assmy, P., Fernández-Méndez, M., Duarte, P., Meyer, A., Randelhoff, A., Mundy, C. J., et al. (2017). Leads in Arctic pack ice enable early phytoplankton blooms below snow-covered sea ice. *Scientific Reports*, *7*(1), 60. http://doi.org/10.1038/srep40850

Bélanger, S., Babin, M., & Tremblay, J.-E. (2013). Increasing cloudiness in Arctic damps the increase in phytoplankton primary production due to sea ice receding. *Biogeosciences*, *10*(6), 4087–4101. http://doi.org/10.5194/bg-10-4087-2013

Carmack, E., Barber, D., Christensen, J., Macdonald, R., Rudels, B., & Sakshaug, E. (2006). Climate variability and physical forcing of the food webs and the carbon budget on panarctic shelves. *Progress in Oceanography*, *71*(2–4), 145–181. http://doi.org/10.1016/j.pocean.2006.10.005

Carmack, E., & Chapman, D. C. (2003). Wind-driven shelf/basin exchange on an Arctic shelf: The joint roles of ice cover extent and shelf-break bathymetry. *Geophysical Research Letters*, *30*(14), 1778. http://doi.org/10.1029/2003GL017526

Cavalieri, D. J., Parkinson, C. L., Gloersen, P., & Zwally, H. (1996). *Sea ice concentrations from Nimbus-7 SMMR and DMSP SSM/I-SSMIS passive microwave data*. Boulder, CO: NASA DAAC at the National Snow and Ice Data Center. http://doi.org/10.5067/8GQ8LZQVL0VL

Chatterjee, S., & Simonoff, J. S. (2013). *Handbook of Regression Analysis*. Somerset, NJ, USA: Wiley Publication.

Cheung, W. W. L., Lam, V. W. Y., Sarmiento, J. L., Kearney, K., Watson, R., Zeller, D., & Pauly, D. (2010). Large-scale redistribution of maximum fisheries catch potential in the global ocean under climate change. *Global Change Biology*, *16*(1), 24–35. http://doi.org/10.1111/j.13652486.2009.01995.x

Codispoti, L. A., Kelly, V., Thessen, A., Matrai, P., Suttles, S., Hill, V., et al. (2013). Synthesis of primary production in the Arctic Ocean: III. Nitrate and phosphate based estimates of net community production. *Progress in Oceanography*, *110*, 126–150. https://doi.org/10.1016/j.pocean.2012.11.006

Crawford, A. D., & Serreze, M. C. (2016). Does the summer Arctic frontal zone influence Arctic Ocean cyclone activity? *Journal of Climate*, *29*, 4977–4993. http://doi.org/10.1175/JCLI-D-15-0755.s1

Dee, D. P., Uppala, S. M., & Simmons, A. J. (2011). The ERA-Interim reanalysis: Configuration and performance of the data assimilation system. *Quarterly Journal of the Royal Meteorological Society*, *137*, 553–597. https://doi.org/10.1002/qj.828

Fer, I., Peterson, A. K., Randelhoff, A., & Meyer, A. (2017). One-dimensional evolution of the upper water column in the Atlantic sector of the Arctic Ocean in winter. *Journal of Geophysical Research: Oceans*, *122*, 1665–1682. http://doi.org/10.1002/2016JC012431

Fichot, C. G., Kaiser, K., Hooker, S. B., Amon, R. M. W., Babin, M., Bélanger, S., et al. (2013). Pan-Arctic distributions of continental runoff in the Arctic Ocean. *Scientific Reports*, *3*(1), 14,485. http://doi.org/10.1038/srep01053

Frey, K. E., Perovich, D. K., & Light, B. (2011). The spatial distribution of solar radiation under a melting Arctic Sea ice cover. *Geophysical Research Letters*, *38*, L22501. http://doi.org/10.1029/2011GL049421

Hátún, H., Azetsu-Scott, K., Somavilla, R., Rey, F., Johnson, C., Mathis, M., et al. (2017). The subpolar gyre regulates silicate concentrations in the North Atlantic. *Scientific Reports*, *7*(1), 14,576–14,289. http://doi.org/10.1038/s41598-017-14837-4

Hays, G. C., Richardson, A. J., & Robinson, C. (2005). Climate change and marine plankton. *Trends in Ecology & Evolution*, *20*(6), 337–344. https://doi.org/10.1016/j.tree.2005.03.004

Hill, V. J. (2008). Impacts of chromophoric dissolved organic material on surface ocean heating in the Chukchi Sea. *Journal of Geophysical Research*, *113*, CO7024. https://doi.org/10.1029/2007JC004119

Hudson, S. R., Granskog, M. A., Sundfjord, A., Randelhoff, A., Renner, A. H. H., & Divine, D. V. (2013). Energy budget of first-year Arctic Sea ice in advanced stages of melt. *Geophysical Research Letters*, *40*, 2679–2683. http://doi.org/10.1002/grl.50517

Huot, Y., Babin, M., & Bruyant, F. (2013). Photosynthetic parameters in the Beaufort Sea in relation to the phytoplankton community structure. *Biogeosciences*, *10*(5), 3445–3454. http://doi.org/10.5194/bg-10-3445-2013

IOCCG (2015). Ocean colour remote sensing in polar seas, edited by M. Babin, et al., IOCCG Report Series, No. 16, International Ocean Colour Coordinating Group, pp. 1–130, Dartmouth, Canada.

Ivanova, N., Pedersen, L. T., Tonboe, R. T., Kern, S., Heygster, G., Lavergne, T., et al. (2015). Inter-comparison and evaluation of sea ice algorithms: Towards further identification of challenges and optimal approach using passive microwave observations. *The Cryosphere*, *9*(5), 1797–1817. http://doi.org/10.5194/tc-9-1797-2015

Jakobson, E., Vihma, T., Palo, T., Jakobson, L., Keernik, H., & Jaagus, J. (2012). Validation of atmospheric reanalyses over the Central Arctic Ocean. *Geophysical Research Letters*, *39*, L10802. http://doi.org/10.1029/2012GL051591

Ji, R., Jin, M., & Varpe, Ø. (2013). Sea ice phenology and timing of primary production pulses in the Arctic Ocean. *Global Change Biology*, *19*(3), 734–741. http://doi.org/10.1111/gcb.12074

Kahru, M., Lee, Z., Mitchell, B. G., & Nevison, C. D. (2016). Effects of sea ice cover on satellite-detected primary production in the Arctic Ocean. *Biology Letters*, *41*(17), 6207–6212. http://doi.org/10.1002/2014GL061047

Kauko, H. M., Pavlov, A. K., Johnsen, G., Granskog, M. A., Peeken, I., & Assmy, P. (2019). Photoacclimation state of an Arctic underice phytoplankton bloom. *Journal of Geophysical Research: Oceans*, *124*, 1750–1762. http://doi.org/10.1029/2018JC014777

Kirillov, S., Dmitrenko, I., Tremblay, B., Gratton, Y., Barber, D., & Rysgaard, S. (2016). Upwelling of Atlantic water along the Canadian Beaufort Sea continental slope: Favorable atmospheric conditions and seasonal and interannual variations. *Journal of Climate*, *29*(12), 4509–4523. http://doi.org/10.1175/JCLI-D-15-0804.1

Kovacs, K. M., Lydersen, C., Overland, J. E., & Moore, S. E. (2010). Impacts of changing sea-ice conditions on Arctic marine mammals. *Marine Biodiversity*, *41*(1), 181–194. http://doi.org/10.1007/s12526-010-0061-0

Kwok, R. (2018). Arctic Sea ice thickness, volume, and multiyear ice coverage: Losses and coupled variability (1958–2018). *Environmental Research Letters*, *13*(10), 105005. http://doi.org/10.1088/1748-9326/aae3ec

Lee, Y. J., Matrai, P. A., Friedrichs, M. A. M., Saba, V. S., Antoine, D., Ardyna, M., et al. (2015). An assessment of phytoplankton primary productivity in the Arctic Ocean from satellite ocean color/in situ chlorophyll-a based models. *Journal of Geophysical Research: Oceans*, *120*, 6508–6541. https://doi.org/10.1002/2015JC011018

Le Fouest, V., Babin, M., & Tremblay, J.-É. (2013). The fate of riverine nutrients on Arctic shelves. *Biogeosciences*, *10*, 3661–3677. http://doi.org/10.5194/bg-10-3661-2013

Lee, S. H., Whitledge, T. E., & Kang, S.-H. (2007). Recent carbon and nitrogen uptake rates of phytoplankton in Bering Strait and the Chukchi Sea. *Continental Shelf Research*, *27*(17), 2231–2249. http://doi.org/10.1016/j.csr.2007.05.009

Lewis, K. M., & Arrigo, K. R. (2020). Ocean color algorithms for estimating chlorophyll a, CDOM absorption, and particle backscattering in the Arctic Ocean. *Journal of Geophysical Research: Oceans*, *125*, e2019JC015706. http://doi.org/10.1029/2019JC015706

Lewis, K. M., Mitchell, B. G., van Dijken, G. L., & Arrigo, K. R. (2016). Regional chlorophyll a algorithms in the Arctic Ocean and their effect on satellite-derived primary production estimates. *Deep Sea Research Part II: Topical Studies in Oceanography*, *130*(c), 14–27. http://doi.org/10.1016/j.dsr2.2016.04.020

Lewis, K. M., van Dijken, G. L., & Arrigo, K. R. (2020). Changes in phytoplankton concentration now drive increased Arctic Ocean primary production. *Science*, *369*(6500), 198–202. http://doi.org/10.1126/science.aay8380

Lien, V. S., Schlichtholz, P., Skagseth, Ø., & Vikebø, F. B. (2017). Wind-driven Atlantic water flow as a direct mode for reduced Barents Sea ice cover. *Journal of Climate*, *30*(2), 803–812. http://doi.org/10.1175/JCLI-D-16-0025.1

Lin, P., Pickart, R. S., Moore, G. W. K., Spall, M. A., & Hu, J. (2019). Characteristics and dynamics of wind-driven upwelling in the Alaskan Beaufort Sea based on six years of mooring data. *Deep Sea Research Part II: Topical Studies in Oceanography*, *162*, 79–92. http://doi.org/10.1016/j.dsr2.2018.01.002

Lindsay, R., Wensnahan, M., & Schweiger, A. (2014). Evaluation of seven different atmospheric reanalysis products in the Arctic. *Journal of Climate*, *27*, 2588–2606. http://doi.org/10.1175/JCLI-D-13

Matsuoka, A., Boss, E., Babin, M., Karp-Boss, L., Hafez, M., Chekalyuk, A., et al. (2017). Pan-Arctic optical characteristics of colored dissolved organic matter: Tracing dissolved organic carbon in changing Arctic waters using satellite ocean color data. *Remote Sensing of Environment*, *200*, 89–101. http://doi.org/10.1016/j.rse.2017.08.009

Matsuoka, A., Hill, V., Huot, Y., Babin, M., & Bricaud, A. (2011). Seasonal variability in the light absorption properties of western Arctic waters: Parameterization of the individual components of absorption for ocean color applications. *Journal of Geophysical Research*, *116*, C02007. http://doi.org/10.1029/2009jc005594

Matsuoka, A., Huot, Y., Shimida, K., Saitoh, S.-I., & Babin, M. (2007). Bio-optical characteristics in the Western Arctic Ocean: Implications for ocean color algorithms. *Canadian Journal of Remote Sensing*, *33*(6), 503–518. https://doi.org/10.5589/m07-059

Meneghello, G., Marshall, J., Timmermans, M.-L., & Scott, J. (2018). Observations of seasonal upwelling and downwelling in the Beaufort Sea mediated by sea ice. *Journal of Physical Oceanography*, *48*(4), 795–805. http://doi.org/10.1175/JPO-D-17-0188.1

Monier, A., Comte, J., Babin, M., Forest, A., Matsuoka, A., & Lovejoy, C. (2014). Oceanographic structure drives the assembly processes of microbial eukaryotic communities. *The ISME Journal*, *9*(4), 990–1002. http://doi.org/10.1038/ismej.2014.197

Mundy, C. J., Gosselin, M., Ehn, J., Gratton, Y., Rossnagel, A., Barber, D. G., et al. (2009). Contribution of under-ice primary production to an ice-edge upwelling phytoplankton bloom in the Canadian Beaufort Sea. *Geophysical Research Letters*, *36*, L17601. http://doi.org/10.1029/2009GL038837

Mundy, C. J., Gosselin, M., Gratton, Y., Brown, K., Galindo, V., Campbell, K., et al. (2014). Role of environmental factors on phytoplankton bloom initiation under landfast sea ice in Resolute Passage, Canada. *Marine Ecology Progress Series*, *497*, 39–49. http://doi.org/10.3354/meps10587

Nishino, S., Kawaguchi, Y., Inoue, J., Hirawake, T., Fujiwara, A., Futsuki, R., et al. (2015). Nutrient supply and biological response to wind-induced mixing, inertial motion, internal waves, and currents in the northern Chukchi Sea. *Journal of Geophysical Research: Oceans*, *119*, 297–312. http://doi.org/10.1002/2013JC009301

Oziel, L., Neukermans, G., Ardyna, M., Lancelot, C., Tison, J.-L., Wassmann, P., et al. (2017). Role for Atlantic inflows and sea ice loss on shifting phytoplankton blooms in the Barents Sea. *Journal of Geophysical Research: Oceans*, *36*, 368. http://doi.org/10.1111/j.1550-7408.1989.tb05528.x

Peng, G., Steele, M., Bliss, A., Meier, W., & Dickinson, S. (2018). Temporal means and variability of Arctic Sea ice melt and freeze season climate indicators using a satellite climate data record. *Remote Sensing*, *10*(9), 1328–1321. http://doi.org/10.3390/rs10091328

Perrette, M., Yool, A., Quartly, G. D., & Popova, E. E. (2011). Near-ubiquity of ice-edge blooms in the Arctic. *Biogeosciences*, *8*(2), 515–524. http://doi.org/10.5194/bg-8-515-2011

Pickart, R. S., Spall, M. A., & Mathis, J. T. (2013). Dynamics of upwelling in the Alaskan Beaufort Sea and associated shelf–basin fluxes. *Deep Sea Research Part I: Oceanographic Research Papers*, *76*, 35–51. http://doi.org/10.1016/j.dsr.2013.01.007

Popova, E. E., Yool, A., Coward, A. C., Aksenov, Y. K., Alderson, S. G., de Cuevas, B. A., & Anderson, T. R. (2010). Control of primary production in the Arctic by nutrients and light: Insights from a high resolution ocean general circulation model. *Biogeosciences*, *7*(11), 3569–3591. http://doi.org/10.5194/bg-7-3569-2010

Pörtner, H.-O., Karl, D., Boyd, P., Cheung, W., Lluch-Cota, S., Nojiri, Y., et al. (2014). Climate change 2014: Impacts, adaptation, and vulnerability. Part A: Global and sectoral aspects. In *Contribution of Working Group II to the Fifth Assessment Report of the Intergovernmental Panel on Climate Change: Ocean Systems* (pp. 411–484). Cambridge, U. K., and New York: Cambridge Univ. press.

Randelhoff, A., Fer, I., & Sundfjord, A. (2017). Turbulent upper-ocean mixing affected by meltwater layers during Arctic summer. *Journal of Physical Oceanography*, *47*(4), 835–853. http://doi.org/10.1175/JPO-D-16-0200.1

Randelhoff, A., Fer, I., Sundfjord, A., Tremblay, J.-É., & Reigstad, M. (2016). Vertical fluxes of nitrate in the seasonal nitracline of the Atlantic sector of the Arctic Ocean. *Journal of Geophysical Research: Oceans*, *121*, 5282–5295. http://doi.org/10.1002/2016JC011779@10.1002/(ISSN)2169-9291.NICE1

Randelhoff, A., & Sundfjord, A. (2018). Short commentary on marine productivity at Arctic shelf breaks: Upwelling, advection and vertical mixing. *Ocean Science*, *14*(2), 293–300. http://doi.org/10.5194/os-14-293-2018

Randelhoff, A., Sundfjord, A., & Reigstad, M. (2015). Seasonal variability and fluxes of nitrate in the surface waters over the Arctic shelf slope. *Geophysical Research Letters*, *42*, 3442–3449. http://doi.org/10.1002/2015GL063655

Renaut, S., Devred, E., & Babin, M. (2018). Northward expansion and intensification of phytoplankton growth during the early ice-free season in Arctic. *Geophysical Research Letters*, *45*, 10,590–10,598. http://doi.org/10.1029/2018GL078995

Rey, F. (2012). Declining silicate concentrations in the Norwegian and Barents seas. *ICES Journal of Marine Science*, *69*(2), 208–212. http://doi.org/10.1093/icesjms/fss007

Reynolds, R. W., Smith, T. M., Liu, C., Chelton, D. B., Casey, K. S., & Schlax, M. G. (2007). Daily high-resolution-blended analyses for sea surface temperature. *Journal of Climate*, *27*, 8221–8228. https://doi.org/10.1175/JCLI-D-14-00293.1

Rogers, J. C. (1997). North Atlantic storm track variability and its association to the North Atlantic oscillation and climate variability of northern Europe. *Journal of Climate*, *10*(7), 1635–1647. https://doi.org/10.1175/1520-0442(1997)010%3C1635:NASTVA%3E2.0.CO;2

Rosel, A., Kaleschke, L., & Birnbaum, G. (2012). Melt ponds on Arctic Sea ice determined from MODIS satellite data using an artificial neural network. *The Cryosphere*, *6*(2), 431–446. https://doi.org/10.5194/tc-6-431-2012

Schulze, L. M., & Pickart, R. S. (2012). Seasonal variation of upwelling in the Alaskan Beaufort Sea: Impact of sea ice cover. *Journal of Geophysical Research*, *117*, C06022. http://doi.org/10.1029/2012JC007985

Schwarz, G. (1978). Estimating the dimension of a model. *The Annals of Statistics*, *6*(2), 461–464. https://doi.org/10.1214/aos/1176344136

Sepp, M., & Jaagus, J. (2010). Changes in the activity and tracks of Arctic cyclones. *Climatic Change*, *105*(3–4), 577–595. http://doi.org/10.1007/s10584-010-9893-7

Serreze, M. C., & Barrett, A. P. (2011). Characteristics of the Beaufort Sea High. *Journal of Climate*, *24*(1), 159–182. http://doi.org/10.1175/2010JCLI3636.1

Serreze, M. C., Barrett, A. P., Crawford, A. D., & Woodgate, R. A. (2019). Monthly variability in Bering Strait oceanic volume and heat transports, links to atmospheric circulation and ocean temperature, and implications for sea ice conditions. *Journal of Geophysical Research: Oceans*, *124*, 9317–9337. http://doi.org/10.1029/2019JC015422

Serreze, M. C., & Barry, R. G. (2011). Processes and impacts of Arctic amplification: A research synthesis. *Global and Planetary Change*, *77*(1–2), 85–96. http://doi.org/10.1016/j.gloplacha.2011.03.004

Serreze, M. C., Carse, F., Barry, R. G., & Rogers, J. C. (1997). Icelandic low cyclone activity: Climatological features, linkages with the NAO, and relationships with recent changes in the Northern Hemisphere circulation. *Journal of Climate*, *10*(3), 453–464. https://doi.org/10.1175/1520-0442(1997)010<0453:ilcacf>2.0.co;2

Serreze, M. C., Crawford, A. D., Stroeve, J. C., Barrett, A. P., & Woodgate, R. A. (2016). Variability, trends, and predictability of seasonal sea ice retreat and advance in the Chukchi Sea. *Journal of Geophysical Research: Oceans*, *121*, 7308–7325. http://doi.org/10.1002/2016JC011977

Serreze, M. C., & Meier, W. N. (2018). The Arctic's sea ice cover: Trends, variability, predictability, and comparisons to the Antarctic. *Annals of the New York Academy of Sciences*, *136*, 250–262. http://doi.org/10.1016/j.pocean.2015.05.001

Smedsrud, L. H., Esau, I., Ingvaldsen, R. B., Eldevik, T., Haugan, P. M., Li, C., et al. (2013). The role of the Barents Sea in the Arctic climate system. *Reviews of Geophysics*, *51*, 415–449. http://doi.org/10.1002/rog.20017

Steele, M., Morison, J., Ermold, W., Rigor, I., Ortmeyer, M., & Shimada, K. (2004). Circulation of summer Pacific halocline water in the Arctic Ocean. *Journal of Geophysical Research*, *109*, C02027. http://doi.org/10.1029/2003JC002009

Stroeve, J. C., Crawford, A. D., & Stammerjohn, S. (2016). Using timing of ice retreat to predict timing of fall freeze-up in the Arctic. *Geophysical Research Letters*, *43*, 6332–6340. http://doi.org/10.1002/2016GL069314

Stroeve, J. C., Serreze, M. C., Holland, M. M., Kay, J. E., Maslanik, J. A., & Barrett, A. P. (2012). The Arctic's rapidly shrinking sea ice cover: A research synthesis. *Climatic Change*, *110*(3–4), 1005–1027. http://doi.org/10.1007/s10584-011-0101-1

Tank, S. E., Manizza, M., Holmes, R. M., McClelland, J. W., & Peterson, B. J. (2011). The processing and impact of dissolved riverine nitrogen in the Arctic Ocean. *Estuaries and Coasts*, *35*(2), 401–415. http://doi.org/10.1007/s12237-011-9417-3

Thomson, J., Fan, Y., Stammerjohn, S., Stopa, J., Rogers, W. E., Girard-Ardhuin, F., et al. (2016). Ocean modelling. *Ocean Modelling*, *105*(C), 1–12. http://doi.org/10.1016/j.ocemod.2016.02.009

Tilinina, N., Gulev, S. K., & Bromwich, D. H. (2014). New view of Arctic cyclone activity from the Arctic system reanalysis. *Geophysical Research Letters*, *41*, 1766–1772. http://doi.org/10.1002/2013GL058924

Timmermans, M.-L., & Marshall, J. (2020). Understanding Arctic Ocean circulation: A review of ocean dynamics in a changing climate. *Journal of Geophysical Research: Oceans*, *125*, e2018JC014378. http://doi.org/10.1029/2018JC014378

Tremblay, J.-É., Bélanger, S., Barber, D. G., Asplin, M., Martin, J., Darnis, G., et al. (2011). Climate forcing multiplies biological productivity in the coastal Arctic Ocean. *Geophysical Research Letters*, *38*, L18604. http://doi.org/10.1029/2011GL048825

Tremblay, J.-É., & Gagnon, J. (2009). The effects of irradiance and nutrient supply on the productivity of Arctic waters: A perspective on climate change. In *Influence of Climate Change on the Changing Arctic and Sub-Arctic Conditions* (Vol. 205, pp. 73–93). Dordrecht: Springer Netherlands. http://doi.org/10.1007/978-1-4020-9460-6_7

Tremblay, J.-É., Michel, C., Hobson, K., Gosselin, M., & Price, N. M. (2006). Bloom dynamics in early opening waters of the Arctic Ocean. *Limnology and Oceanography*, *51*(2), 900–912. https://doi.org/10.4319/lo.2006.51.2.0900

Tremblay, J.-É., Raimbault, P., Garcia, N., Lansard, B., Babin, M., & Gagnon, J. (2014). Impact of river discharge, upwelling and vertical mixing on the nutrient loading and productivity of the Canadian Beaufort Shelf. *Biogeosciences*, *11*(17), 4853–4868. http://doi.org/10.5194/bg-11-4853-2014

Tremblay, J.-É., Simpson, K., Martin, J., Miller, L., Gratton, Y., Barber, D., & Price, N. M. (2008). Vertical stability and the annual dynamics of nutrients and chlorophyll fluorescence in the coastal, southeast Beaufort Sea. *Journal of Geophysical Research*, *113*, C07S90. http://doi.org/10.1029/2007JC004547@10.1002/(ISSN)2169-9291.CASES1

Uchimiya, M., Motegi, C., Nishino, S., Kawaguchi, Y., Inoue, J., Ogawa, H., & Nagata, T. (2016). Coupled response of bacterial production to a wind-induced fall phytoplankton bloom and sediment resuspension in the Chukchi Sea Shelf, Western Arctic Ocean. *Frontiers in Marine Science*, *3*, 533. http://doi.org/10.3389/fmars.2016.00231

Vavrus, S. J. (2013). Extreme Arctic cyclones in CMIP5 historical simulations. *Geophysical Research Letters*, *40*, 6208–6212. http://doi.org/10.1002/2013GL058161

Vetrov, A. A., Romankevich, E. A., & Belyaev, N. A. (2008). Chlorophyll, primary production, fluxes, and balance of organic carbon in the Laptev Sea. *Geochemistry International*, *46*(10), 1055–1063. http://doi.org/10.1134/S0016702908100091

Wang, J., Cota, G. F., & Comiso, J. C. (2005). Phytoplankton in the Beaufort and Chukchi seas: Distribution, dynamics, and environmental forcing. *Deep Sea Research Part II: Topical Studies in Oceanography*, *52*(24–26), 3355–3368. http://doi.org/10.1016/j.dsr2.2005.10.014

Wassmann, P., Duarte, C. M., Agustí, S., & Sejr, M. K. (2011). Footprints of climate change in the Arctic marine ecosystem. *Global Change Biology*, *17*(2), 1235–1249. http://doi.org/10.1111/j.1365-2486.2010.02311.x

Wassmann, P., Slagstad, D., & Ellingsen, I. (2010). Primary production and climatic variability in the European sector of the Arctic Ocean prior to 2007: Preliminary results. *Polar Biology*, *33*(12), 1641–1650. http://doi.org/10.1007/s00300-010-0839-3

Williams, W. J., & Carmack, E. C. (2008). Combined effect of wind-forcing and isobath divergence on upwelling at Cape Bathurst, Beaufort Sea. *Journal of Marine Research*, *66*(5), 645–663. http://doi.org/10.1357/002224008787536808

Williams, W. J., & Carmack, E. C. (2015). The "interior" shelves of the Arctic Ocean: Physical oceanographic setting, climatology and effects of sea-ice retreat on cross-shelf exchange. *Progress in Oceanography*, *139*, 24–41. http://doi.org/10.1016/j.pocean.2015.07.008

Woodgate, R. A. (2018). Increases in the Pacific inflow to the Arctic from 1990 to 2015, and insights into seasonal trends and driving mechanisms from year-round Bering Strait mooring data. *Progress in Oceanography*, *160*, 124–154. http://doi.org/10.1016/j.pocean.2017.12.007

Woodgate, R. A., Aagaard, K., & Weingartner, T. J. (2005). Monthly temperature, salinity, and transport variability of the Bering Strait through flow. *Geophysical Research Letters*, *32*, L04601. http://doi.org/10.1029/2004GL021880

Yim, B. Y., Min, H. S., Kim, B.-M., Jeong, J.-H., & Kug, J.-S. (2016). Sensitivity of Arctic warming to sea ice concentration. *Journal of Geophysical Research: Atmospheres*, *121*, 6927–6942. http://doi.org/10.1002/2015JD023953

Zahn, M., Akperov, M., Rinke, A., Feser, F., & Mokhov, I. I. (2018). Trends of cyclone characteristics in the Arctic and their patterns from different reanalysis data. *Journal of Geophysical Research: Atmospheres*, *123*, 2737–2751. http://doi.org/10.1002/2017JD027439

Zhang, J., Ashjian, C., Campbell, R., Hill, V., Spitz, Y. H., & Steele, M. (2014). The great 2012 Arctic Ocean summer cyclone enhanced biological productivity on the shelves. *Journal of Geophysical Research: Oceans*, *119*, 297–312. http://doi.org/10.1002/2013JC009301

Zhang, J., Spitz, Y. H., Steele, M., Ashjian, C., Campbell, R., Berline, L., & Matrai, P. (2010). Modeling the impact of declining sea ice on the Arctic marine planktonic ecosystem. *Journal of Geophysical Research*, *115*, C10015. http://doi.org/10.1029/2009JC005387